An Application of Neural Networks for Image Reconstruction in Electrical Capacitance Tomography Applied to Oil Industry

Norberto Flores[1], Ángel Kuri-Morales[2], and Carlos Gamio[3]

[1] Instituto Mexicano del Petróleo, Eje Central Lázaro Cárdenas 152, San Bartolo Atepehuacan 07730, Distrito Federal, México
nfloresg@imp.mx
http://www.imp.mx
[2] Instituto Tecnológico Autónomo de México, Río Hondo 1, Progreso Tizapán 01080, Distrito Federal, México
akuri@itam.mx
http://www.itam.mx
[3] Glasgow Caledonian University, 70 Cowcaddens Road, Glasgow G4 0BA United Kingdom
carlos.gamio@gcal.ac.uk
http://www.gcal.ac.uk

Abstract. The article presents a possible solution to a typical tomographic images generation problem from data of an industrial process located in a pipeline or vessel. These data are capacitance measurements obtained non-invasively according to the well known ECT technique (Electrical Capacitance Tomography). Every 313 pixels image frame is derived from 66 capacitance measurements sampled from the real time process. The neural nets have been trained using the backpropagation algorithm where training samples have been created synthetically from a computational model of the real ECT sensor. To create the image 313 neuronal nets, each with 66 inputs and one output, are used in parallel. The resulting image is finally filtered and displayed. The different ECT system stages along with the different tests performed with synthetic and real data are reported. We show that the image resulting from our method is a faster and more precise practical alternative to previously reported ones.

1 Introduction

Process tomography consists of obtaining images from the inside of pipelines, reactors or other type of containers that are part of industrial processes [1] [4]. Such visualization is performed non-invasively. There are several techniques for obtaining images, depending on the type of measurement used (acoustic, magnetic resonance, electrical, etc.). One way is to obtain capacitance measurements according to the ECT technique [1] [3].

Image reconstruction techniques from Artificial Neural Nets (ANN) trained by means of a supervised learning algorithm, require large number of samples (capacitance measurements for several known permittivity distributions) to be trained.

J.F. Martínez-Trinidad et al. (Eds.): CIARP 2006, LNCS 4225, pp. 371 – 380, 2006.

Because of the difficulty in obtaining such examples experimentally, we need to develop a methodology which allows us to generate synthetic examples from a real-sensor model.

From the set of generated samples the ANN is trained assuming the capacitance information as the input and the permittivity distribution information as the output. The ANN thusly trained has the capability to respond to new sensor data, giving adequate permittivity distribution which allows us to reconstruct a tomographic image.

1.1 Electrical Capacitance Tomography

ECT is an innovating technique (late 80s) [1] [10] for industrial multiphase process visualization, suitable for electrically insulating materials. Its potential applications in the petroleum industry [4] range from multiphase flow measurement and monitoring in producing wells to separator and fluidized bed optimization [2].

The ECT technique consists in placing an electrode array around a pipeline or vessel made of an insulating material that contains the process to be visualized. By using the adequate tools, the capacitances between all possible electrode pairs needs to be measured [6]. The obtained readings depend on the dielectric constant value (electrical permittivity) of the different phases or components of the mixture and the way they are distributed inside the pipeline or vessel. The next step is to obtain an image of such distribution from the measured capacitance data by means of an adequate image reconstruction algorithm. Figure 1 shows a schematic diagram of an ECT system with its main components. Besides the capacitance sensor, a basic ECT system is made up with a data acquisition system and a computer for image reconstruction [10].

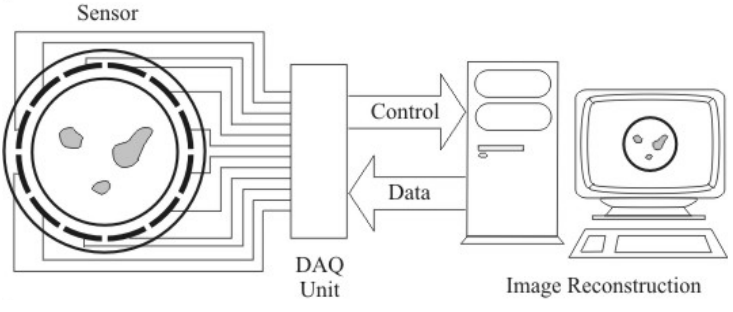

Fig. 1. ECT system components

2 ECT Sensor Used

The number and the size of electrodes depend on the specific application. Most of the applications developed until now make use of sensors with 8, 12, or 16 electrodes [1] [3] [6], they must be inside a grounded screen to cut down noise and the influence of external fields (see Fig 2). Besides, the sensor used has two grounded cylindrical end guards to eliminate the changes on the electric field borders.

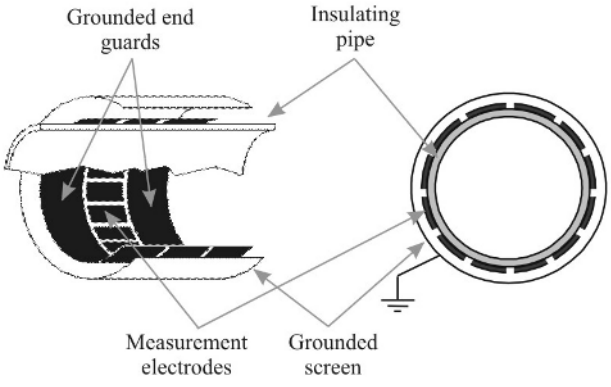

Fig. 2. ECT Sensor Schematic Diagram

The sensor from the Mexican Petroleum Institute used in this research has 12 electrodes (see Fig. 3a), so it is possible to measure 66 capacitance values between them (see Figure 3b). These capacitances are extremely small and, due to this, very sensitive measurement circuits are needed. Such values are in the 0.1 to 500 femtofarads range (1 femtofarad = 10 e-15 farads).

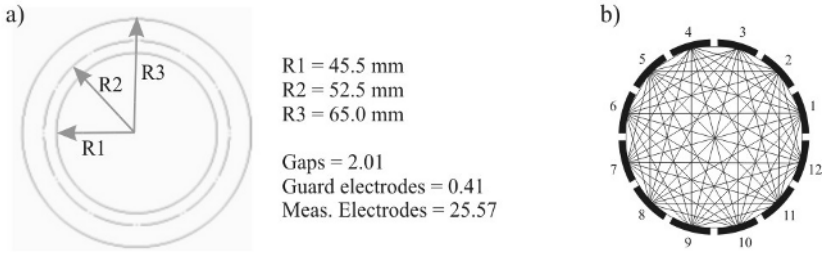

Fig. 3. Mexican Institute of Petroleum ECT Sensor. a) Dimensions, b) 66 electrode-pair combinations

2.1 Numeric ECT Sensor Model

Although the sensor is a three-dimensional device, it is possible to use a two dimension model due to the fact that it is representative of a central transversal section. The natural deformation of the electric field at the edges of the pipe formed by the measurement electrodes is controlled by means of the grounded electrodes placed in both edges (see Figure 2). Apart from the insulating pipe, measurement electrodes, guard electrodes and shielded screen dimensions, the model geometry includes the spatial discretization of the inner part of the sensor (R1 in Figure 3). It has been discretizated into 313 uniform size zones, as shown in Figure 4.

The model allows us to have a method from which numerical calculation can be carried out for the electric potential ϕ in the space of the sensor. This is necessary as

an intermediate step towards the capacitance calculation. An ECT sensor can be considered as an electrostatic field problem. The electric potential ϕ within the sensor [3] is calculated by solving the following second order partial differential equation

$$\nabla \cdot [\varepsilon(x,y)\nabla\phi(x,y)] = 0 \tag{1}$$

where $\phi(x,y)$ is the potential distribution in two dimensions, and $\varepsilon(x,y)$ is the relative permittivity distribution in two dimensions.

To complete the model, the boundary conditions (Dirichlet boundary conditions) related to the measurement technique are shown in (2). When electrode i is the excitation electrode, such conditions are:

$$\psi_i = \begin{cases} V_{exc} & (x,y) \subseteq \Gamma_i \\ 0 & (x,y) \subseteq \Gamma_j \quad (j = 1, \ldots, n;\ j \neq i) \quad and \quad (x,y) \subseteq (\Gamma_s + \Gamma_g) \end{cases} \tag{2}$$

where Γ_i is the spatial location of the measurement (excitation) electrode; Γ_j is the spatial location of the 11 detecting electrodes; Γ_s the one of the sensor screen; and Γ_g the one of the 12 grounded guard electrodes placed between the 12 measurement electrodes.

The sensor model will be used to simulate a real sensor. This means that it will be able to solve the ECT forward problem calculating capacitances between all possible electrode pairs. To achieve this, equation (1) has to be solved first such that the potential distribution $\phi(x,y)$ is obtained within the sensor.

One way to calculate $\phi(x,y)$ is through the finite element method (FEM) [7]. Using this method, an approximation to the potential ϕ will be obtained in the sensor at a finite set of points corresponding to the nodes of the triangular mesh that is normally used in the finite element method.

Once the potential distribution is found within the sensor, the electric charge Q_j on each detector electrode is calculated by using Gauss law

$$Q_j = \oint_{\Gamma_j} (\varepsilon(x,y)\nabla\phi(x,y)\cdot\mathbf{n})\mathrm{d}s \tag{3}$$

where Γ_j is a closed curve surrounding the detector electrode and $\mathbf{n}$ is the normal vector along the Γ_j.

Finally the capacitance can be computed by an energy method, the energy required to charge a capacitor is given by the expression

$$W_e = \frac{Q^2}{2C} \tag{4}$$

which is equal to the energy of the electrostatic field. So the capacitance is easily obtained from (5).

$$C = \frac{Q^2}{2W_e} \tag{5}$$

3 ANN Solution's Description

The tomography problem is, mathematically speaking, an inverse problem, since from the observed effects (the change in magnitude of capacitances) our aim is to obtain the causes which originate them (material distribution in the inner part of the sensor). The solution of an inverse problem, for our ECT case, consists on obtaining the discretized permittivity distribution $\boldsymbol{\varepsilon}$ ($\boldsymbol{\varepsilon} = \{\varepsilon_1, \varepsilon_2, .. , \varepsilon_{313}\}$) starting from the set of capacitance measurements, represented by the $\mathbf{c}$ vector ($\mathbf{c} = \{c_1, c_2, .. , c_{66}\}$).

$$\begin{aligned} \varepsilon_1 &= f_1(c_1, c_2, c_3, ..., c_{66}) \\ \varepsilon_2 &= f_2(c_1, c_2, c_3, ..., c_{66}) \\ &\vdots \\ \varepsilon_{313} &= f_{313}(c_1, c_2, c_3, ..., c_{66}) \end{aligned} \tag{6}$$

As mentioned before, an ECT process consists of two stages: 1) capacitances obtained in a specific moment; 2) image construction (see Fig. 4). This last stage has been implemented by using an ANN.

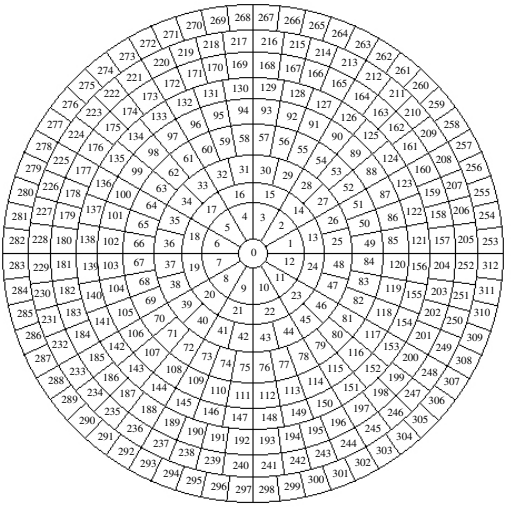

Fig. 4. Pixels distribution that forms the tomographic image

Multilayer Perceptron is the ANN selected type as they are universal function aproximators for a nonlinear input-output mapping [5]. An MLP is used to solve each of the 313 f_p functions (with p= 1, … , 313) obtaining $\boldsymbol{\varepsilon}$.

In the image creation stage, $\mathbf{c}$ is input by several ANNs (see Fig. 5) calculating individually the ε_p pixel values. As a result each pixel is assigned a 1-3 permittivity value corresponding to a substances mixture (For instance, petroleum will have a permittivity close to 3; gas will have a value close to 1; while in the case of a mixture,

an intermediate value will be observed). Afterwards, the pixel value will be mapped to the range [0-255] that corresponds to its final gray level (represented with 8 bits).

3.1 Use of Neural Networks in the Image Reconstruction Stage

The ANNs are now grouped in a module: Its full architecture consists of 313 ANNs in parallel (see Fig. 5). Vector **c** is fed and the module outputs the corresponding **ε** vector. Therefore, **ε** represents permittivity distribution in the sensor transversal section. The image is made up according to the pixel numbers as shown in Figure 4.

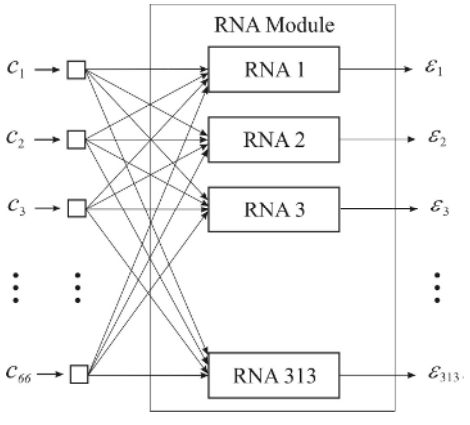

Fig. 5. RNA module for solving the TCE problem

For each ε_p pixel calculation identical ANNs are used: one per pixel. Its architecture is 66-4-7-1 (see Fig. 6), meaning 66 inputs; a first hidden 4 neuron layer, a second 7 neuron one, and a unique neuron in the output layer supplying the permittivity value for ε_p.

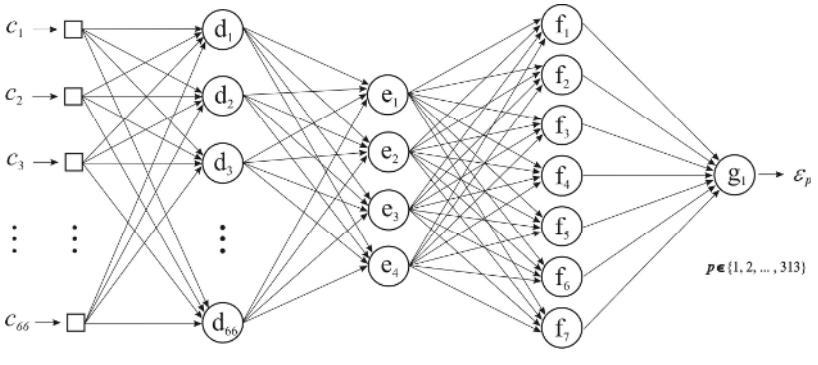

Fig. 6. ANN Architecture

These ANNs have been trained by using the traditional backpropagation algorithm. 1000 training and 150 test examples have been created to achieve such training. Examples are created in the following manner: a p pixel discretized permittivity distribution is chosen. Such distribution makes up vector $\boldsymbol{\varepsilon}$ which is then fed to the computational sensor model to get n capacitances making up $\mathbf{c}$ vector. Later on, both are merged resulting into a training or test example as shown in Figure 7. These items of the sample have 379 elements for p=313 and n=66.

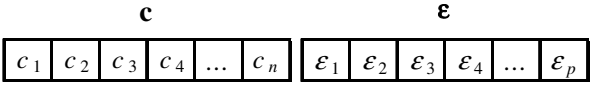

Fig. 7. Examples structure for training and test

A large majority of these examples were randomly generated. 100 training examples were created by using known distribution patterns of materials in the flow, such as: stratified, annular and with bubbles. Training was performed for 1500 epochs, reaching a 0.19 training error, and a 0.24 testing error. A 0.1 learning rate has been used for the three computational layers. Also, a 0.1 momentum constant has been used in them.

4 ANN Recall and Digital Image Processing Module

The general method's performance is now described. As mentioned before capacitance values are in order of femtofarads. Vector $\mathbf{c}$ is normalized in the [0, 1] interval, and input the trained ANN module. A normalized permittivity value is obtained in [0, 1] at the module output. Such a value is now denormalized and a grey level value (from 0 to 255) is displayed as the output value in the corresponding pixel.

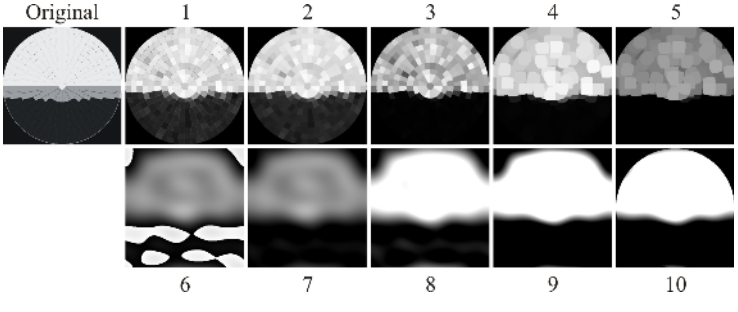

Fig. 8. Digital Image Processing steps

Finally the image made up with the 313 pixel aggregate is passed through a Digital Image Processing (DIP) module mainly to get dissemination among the pixels to present a tomographic aspect image. The DIP module is made up by

applying a ten step sequence (see Figure 8) as follows: 1) Circular mask to eliminate the four black corners, outside the circle, from the treatment; 2) Median filter to add blur (slight fading at the edges between the pixels); 3) A lookup table (LUT) 1/x type, with x= 0.4, for a better brightness, turning the darker zones into even darker ones; 4) Dilation of the light zones; 5) Decreasing brightness; 6) Low pass FFT Filter (Consisting of three steps: a) Finding the FFT, b) Filtering low frequencies from the resulting images and, c) Going back to the image dominium by means of the inverse FFT); 7) Noise elimination from the saturation zones in the former step (The noise is inverted and then subtracted from itself); 8) The image is added to itself to double the gray level from the light parts to recover the brightness withdrawn in 3 and 5 steps; 9) Brightness and contrast are adjusted; 10) A circular mask (as in step one) is applied again.

5 Test Using Synthetic Data for Validation

The process for 4 synthetic images is described in what follows. Both the ANN and the DIP module results are shown. First the desired image (original image) is defined and put in $\boldsymbol{\varepsilon}$ form. Later the ECT sensor model is used to get the corresponding $\mathbf{c}$ vector. Then $\mathbf{c}$ and $\boldsymbol{\varepsilon}$ are merged and RNA module is used to simulate ECT system performance. Finally, the resulting images are passed by the DIP module. The results can be easily validated. Figure 9 displays the ANN module's output and results after applying DIP.

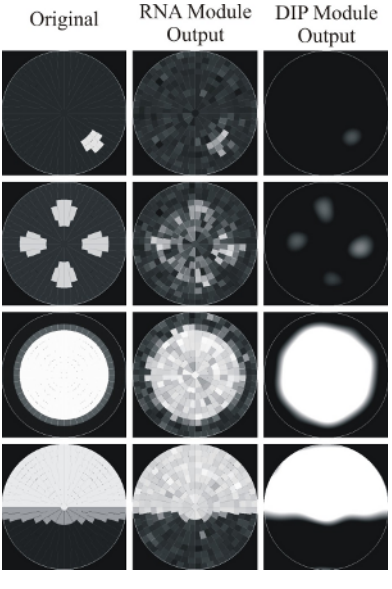

Fig. 9. Original Synthetic Images versus generated ones by using the ECT system

These results show that the ANN method effectively yields satisfactory results for tomographic images reconstruction from capacitance measurements. The light zones represent gas zones (permittivity close to 1), while the dark zones represent oil (permittivity close to 3). All the examples were integrated with different permittivity values; examples 3 and 4 have three different levels, representing oil, foam and gas. The first two examples represent a pipeline filled with oil with 1 and 4 gas bubbles respectively.

6 Experiments Using Real Data

Results from tests performed with real data from a petroleum reservoir simulator are now shown. Real gas and oil at different pressures and amounts were passed through the sensor.

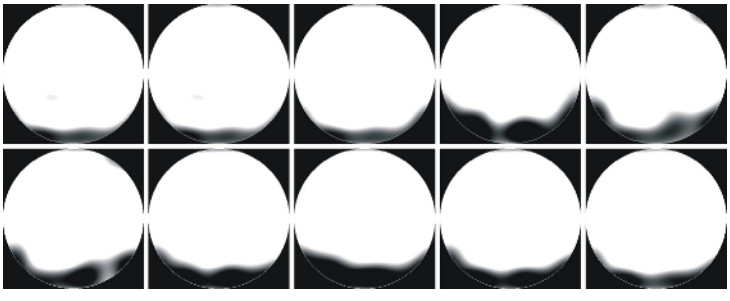

Fig. 10. Experiment using gas and oil. Frames were acquired at 10 ms intervals

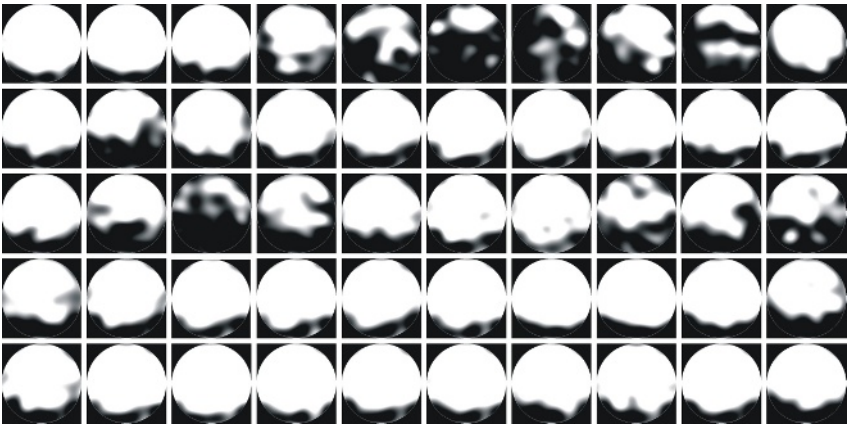

Fig. 11. Experiment using gas and oil. Frames were acquired at 10 ms intervals

Figures 10 and 11 show tomographic images obtained from two experiments. Figure 10 shows an experiment with 0.246 million scfd (standard cubic feet per day) for gas and 182.37 bpd (barrels per day) for oil, having a mixture pressure of 5.5 barbg

(barg gauge). Experiment in Figure 11 was carried out with 0.248 million scfd and 2,263.33 bpd, making a 5.7 barbg pressure.

7 Conclusions

The ANN is a proven functional method for ECT image reconstruction. Several worldwide researchers have already reported promissory results by using this technique [8] [9] [11]. Experiments displayed in this paper have reached 0.24 maximum error image results. This can be measured only when testing known synthetic patterns. Error measurements from real data cannot be supplied because the transversal distribution reference from different flow phases going through a pipe is unknown. And it is precisely here where our method is most useful. The proven effectiveness of the ANN model capabilities allows us to extrapolate the observed and known results to unknown areas of operation, thus fulfilling the original aim of accurately modeling the phenomenon under study.

References

1. Beck, M., Byars, M., Dyakowski, T., Waterfall, R., He, R., Wang, S. J., Yang, W. Q.: Principles and industrial applications of electrical capacitance tomography. Measurement + Control, Vol. 30 (1997) 197–200.
2. Dyakowski T., Jeanmeure, L. F., Jaworski, A. J.: Applications of electrical tomography for gas-solids and liquid-solids flows – A review. Powder technol, Vol. 112 (2000) 174–192.
3. Gamio, J. C., Ortiz-Alemán, C.: An interpretation of the Linear Back-Projection Algorithm Used in Capacitance Tomography. 3rd World Congress on Industrial Process Tomography. Bannf (2003) 427-432.
4. Hammer, E. A., Johansen, G.: A Process tomography in the oil industry – State of the art and future possibilities. Measurement + Control. Vol. 3 (1997) 11-14.
5. Hecht-Nielsen, R.: Kolmogorov's mapping neural network existence theorem. First IEEE International Conference on Neural Networks. Vol. 30 (1987) 212-216.
6. Huang, S. M., Xie, C. G, Thorn, R., Snowen, D., Beck, M. S.: Design of sensor electronics for electrical capacitance tomography. IEE Proc. G. Vol. 139 (1992) 83-88.
7. Khan, S. H. y Abdullah, F.: Finite element modeling of multielectrode capacitive systems for flow imaging. IEE Proceedings-G. Vol. 140(3) (1993) 216-222.
8. Nooralahiyan, A. Y., Hoyle, B., Bailey, N.: Neural network for pattern association in electrical capacitance tomography. IEE Proc.-Circuits Devices Syst. Vol. 141(6) (1994) 517-521.
9. Sun, T. D., Mudde, R., Schouten, J.C., Scarlett, B., van den Bleek, C.M.: Image reconstruction of an electrical capacitance tomography system using an artificial neural network. 3rd World Congress on Industrial Process Tomography. Buxton 1999) 174-180.
10. Yang, W. Q., Peng, L.: Image reconstruction algorithms for electrical capacitance tomography – Review Article. Measurement Science and Technology. Vol. 14 (2003) R1 – R13.
11. Warsito, W., Fan, L-S.: Neural network based multi-criterion optimization image reconstruction technique for imaging two- and three-phase flow systems using electrical capacitance tomography. Measurement Science and Technology. Vol. 12 (2001) 2198 – 2210.